ELSEVIER

Contents lists available at ScienceDirect

Earth and Planetary Science Letters

journal homepage: www.elsevier.com/locate/epsl





Limited water contents of wadsleyite and ringwoodite coexisting with hydrous minerals in cold subducting slabs

Takayuki Ishii ^{a,b,c,*}, Jintao Zhu ^{a,d}, Eiji Ohtani ^e

- ^a Institute for Planetary Materials, Okayama University, Misasa 682-0193, Japan
- ^b Bayerisches Geoinstitut, University of Bayreuth, Universitätsstraße 30 95447 Bayreuth, Germany
- ^c Center of High Pressure Science and Technology Advanced Research (HPSTAR), Beijing 100094, China
- ^d School of Earth and Space Sciences, Peking University, Beijing 100871, China
- e Department of Earth Sciences, Graduate School of Science, Tohoku University, Sendai, Miyagi 980-8578, Japan

ARTICLE INFO

Key words: Subducting slab Water Olivine Ringwoodite Hydrous phase Earthquake

ABSTRACT

How water is distributed in a subducting slab is essential to understand water transport into the deep mantle and mechanisms of deep-focus earthquakes and slab deformation around the 660-km discontinuity. A recent experimental study demonstrated that water contents of olivine and wadsleyite coexisting with hydrous phase A is limited at upper mantle pressures, suggesting strong water partitioning to the hydrous phase. However, water distribution between nominally anhydrous and hydrous minerals at the deeper mantle is not investigated in detail. We determined water contents in wadsleyite and ringwoodite coexisting with hydrous phases down to transition-zone depths along cold slab temperatures. Wadsleyite coexisting with hydrous phase A has \sim 200 ppm water at 14–16 GPa and 800 °C. At 21 GPa, ringwoodite coexisting with superhydrous phase B has 8–13 ppm water at 800 °C and 46 ppm at 900 °C. Thus, olivine and its high-pressure polymorphs are kinetically dry along cold slab core conditions even in a wet subducting slab. Slab deformation and stagnation around 660 km depth can be caused by grain-size reduction due to phase transitions of dry olivine and the presence of rheologically weak hydrous phases. The deepest earthquakes below 660 km depth can be caused by dehydration of hydrous phases.

1. Introduction

Water, transported into the mantle by nominally anhydrous (NAMs) and hydrous minerals in subducting slabs, plays important roles in chemical evolution and dynamics of the mantle. For example, water in olivine enhances its deformation due to hydrolytic weakening (Karato and Jung, 2003; Mei and Kohlstedt, 2000) and transformation kinetics (Kubo et al., 1998). Such effects can control dynamic processes during slab subduction.

Olivine, the most abundant mineral in the Earth's upper mantle, transforms to high-pressure polymorphs of wadsleyite and ringwoodite at depths of 410 km and 520 km, respectively, consisting of the mantle transition zone (e.g. Irifune, 1994; Irifune and Isshiki, 1998; Ishii et al. 2018a). On the other hand, the olivine transformations are delayed in the cold interiors of subducting slabs because slab temperature is not enough to activate the phase transitions (Perrillat et al. 2016; Sung and Burns, 1976). In fact, the presence of such metastable olivine has been

seismologically observed as low-velocity anomalies in cold cores of some slabs down to 580–630 km deep (Iidaka and Suetsugu, 1992; Jiang et al., 2008), which have been called metastable olivine wedges. The phase transformation of olivine in the metastable olivine wedge is generally considered to be the cause of deep-focus earthquakes (Green and Houston, 1995; Kirby et al., 1991).

Water contents of olivine and its high-pressure polymorphs are key to understand hydration state of subducting slabs. Olivine, wadsleyite, and ringwoodite can store up to 0.9, 3.1, and 2.7 wt.% of water, respectively, under water-saturated conditions (e.g. Inoue et al. 1995; Kohlstedt et al., 1996; Smyth et al., 2006). Most studies focused on solubility of water in these minerals along temperatures where hydrous melt coexists (e.g. $>1200\,^{\circ}$ C). However, the inner part of subducting slabs is under much lower temperatures (e.g. Kirby et al. 1996) and therefore hydrous minerals can appear in the region. Our recent experimental study demonstrated that olivine and wadsleyite coexisting with hydrous phase A contain limited water in their crystal structures at

E-mail address: takayuki.ishii@okayama-u.ac.jp (T. Ishii).

^{*} Corresponding author.

pressures of 8–12 GPa corresponding to upper mantle depths and temperatures of 700–900 °C (Ishii and Ohtani, 2021; Ohtani and Ishii, 2024). Their study thus showed strong water partitioning to hydrous phase A in cold subducting slabs, requiring reconsideration of the hydration state of subducting slabs. To understand the hydration state in more detail, water contents of wadsleyite and ringwoodite coexisting with hydrous phases are required in deep mantle conditions.

In this study, we determined water contents of wadsleyite and ringwoodite coexisting with hydrous phases under water-undersaturated conditions (no additional hydrous fluid/melt) up to 21 GPa using a multi-anvil press. We also conducted phase-equilibrium experiments using hydrous wadsleyite and ringwoodite to robustly confirm stability of hydrous phases and constrain water contents of wadsleyite and ringwoodite in the pressure-temperature range. Based on the water content of these phases, we discuss the hydration state of the subducting slab, origin of deep-focus earthquakes, and slab dynamics.

2. Experimental method

2.1. Starting materials and capsule configuration for water partitioning experiments

Water partitioning between olivine polymorphs and hydrous minerals was examined by the method used in Ishii and Ohtani (2021). Wadsleyite single crystals or ringwoodite polycrystal aggregates were packed in a welded-gold capsule together with a hydrous silicate powdered mixture which becomes wadsleyite + hydrous phase A+ clinoenstatite and ringwoodite + superhydrous phase B+ stishovite after experiments, respectively. The detailed information of sample syntheses and capsule configurations for these experiments are described below.

Two kinds of single crystals of Mg₂SiO₄ wadsleyite with slightly different water contents (121 and 361 ppm) were prepared at 18 GPa and 1800 °C for 3 h (Table 1). The wadsleyite crystals with the lower water content were synthesized using an Mg₂SiO₄ forsterite (Fo) powder synthesized by Ishii et al. (2018b; 2019a) that was kept in a vacuuming furnace at 80 °C for >1 day just before packing in a rhenium capsule. This sample capsule was immediately assembled and compressed to the desired pressure to minimize absorption of water from the air. On the other hand, wadsleyite with the higher water content was prepared with the Fo powder that was kept in the air for >1 day just before packing in the rhenium capsule to obtain the slightly higher water content in wadslevite. Hydrous silicate powdered mixtures were prepared as Fo: $[2Mg(OH)_2 \text{ brucite (Br)} + SiO_2 \text{ quartz (Qz)}] = 8:2 \text{ (mole) including a}$ water content of \approx 4.9 wt.% (8Fo+2[2Br+Qz]). The synthesized single crystals with $\sim 200 \, \mu m$ were picked up and packed in the center of a gold capsule. The sample capsule was filled out by the hydrous powdered mixture. The gold capsule was welded shut to avoid escaping water during high-pressure experiment.

Two kinds of ringwoodite polycrystal aggregates with ${\sim}1$ ppm and 231 ppm were also prepared at 21 GPa and 1700 °C and 1400 °C, respectively (Table 1). In the same manner as the wadsleyite syntheses mentioned above, we used the Fo powder for >1 day kept in the vacuuming furnace at 80 °C and in the air before packing into rhenium capsules. The recovered ringwoodite is polycrystalline based on X-ray diffraction (XRD) study but transparent. The aggregate was cut into several fragments with dimensions of ${\sim}200~\mu m$. The aggregate was put in the center of a gold capsule. The space inside the capsule was filled out by a hydrous powdered mixture of Fo: [2Br + Qz] = 9:1(mole) including a water content of ${\approx}2.5$ wt.% (9Fo+1[2Br+Qz]). The gold capsules were also welded shut.

2.2. Starting materials for experiments using highly hydrated olivine polymorphs

To confirm stable phases, we also conducted experiments using

Table 1 Experimental conditions and results.

Run #	Starting material [†]	P	T	D	Phase	Water content
		GPa	°C	h		ppm wt*
1k3856	Fo	18	1800	3	d-Wd	121(12)
H842	Fo	18	1800	3	h-Wd	361(13)
H894	Fo+5 wt% H_2O	15	1300	2	hh-Wd+Melt	20,008
						(4156)
S7475	Fo	23	1700	3	d-Rw	<1§
1k3857	Fo	21	1400	3	h-Rw	231(32)
5k4025	Fo+5 wt%H ₂ O	20	1400	2	hh-Rw+Melt	16,361
						(2000)
H879	h-Wd/8Fo+2	14	800	26	Wd+PhA+Cen [‡]	222(13)
	$[Br+Qz]^{\dagger}$					
1k3860	#1:h-Wd/	16	800	24	Wd+PhA+Cen [‡]	213(20)
	8Fo+2					
	$[Br+Qz]^{\dagger}$					
	#2:d-Wd/	16	800	24	Wd+PhA+Cen [‡]	244(28)
	8Fo+2					
	$[Br+Qz]^{\dagger}$					
1k3921	#1:d-Rw/	21	800	28	Rw+sPhB+St [‡]	8(9)
	9Fo+1					
	$[Br+Qz]^{\dagger}$					
	#2:h-Rw/	21	800	28	$Rw+sPhB+St^{\ddagger}$	13(6)
	9Fo+1					
	$[Br+Qz]^{\dagger}$					
1k3726	d-Rw/9Fo+1	21	900	26	Rw+sPhB+St [‡]	46(18)
	$[Br+Qz]^{\dagger}$					
H934	hh-Wd	12	800	24	Wd+PhA+Cen	_
5k4053	hh-Rw	20	800	20	Rw+sPhB+St	_

Annotations: Fo, forsterite; Wd, wadsleyite; Rw, ringwoodite; Cen, clinoenstatite; PhA, hydrous phase A; sPhB, superhydrous phase B; St, stishovite Br, brucite; Qz, quartz; d-Wd, nearly dry wadsleyite; h-Wd, slightly hydrated wadsleyite; hh-Wd, highly hydrated wadsleyite; d-Rw, dry ringwoodite; h-Rw, slightly hydrated ringwoodite; hh-Rw, highly hydrated ringwoodite.

* Average water contents determined with the calibration of Bolfan-Casanova et al. (2018). Each estimated value is shown in Table S1 and S2.

- † Starting materials of wadsley ite or ringwoodite single phase / hydrous powered mixture part.
- [‡] Phases recovered of hydrous powered mixture parts.
- § OH peaks were not detected.

highly hydrated olivine polymorphs. We call these experiments phase-equilibrium experiments hereafter. Hydrous wadsleyite and ring-woodite with 2.0 and 1.6 wt.% water, respectively, were first synthesized at 15 GPa and 1300 °C and 20 GPa and 1400 °C for 2 h. The starting material was a mixture of reagent-grade Mg(OH)2, MgO, and SiO2 in proportions identical to Mg2SiO4 $+\,5\,$ wt.%H2O. Several synthesized single crystals were put in a welded gold capsule for the phase-equilibrium experiments.

2.3. High pressure-temperature experiment

We used several multi-anvil presses: the 1000-ton Kawai-type multianvil press installed at the Bayerisches Geoinstitut, University of Bayreuth (BGI), and the 6-axis multi-anvil press and 1000-ton and 5000-ton Kawai-type multi-anvil presses at the Institute for Planetary Materials, Okayama University (IPM). Except for the synthesis of dry ringwoodite with \sim 1 ppm water, which was conducted at BGI, all experiments were conducted using multi-anvil presses at IPM. High-pressure experiments were conducted using Cr-doped MgO pressure media with a 10-mm edge length in combination with tungsten carbide (WC) anvils with a 4-mm truncated edge length. Concepts of the cell assembly used in this study are the same as Ishii and Ohtani (2021). A cylindrical LaCrO₃ heater was adopted as a heater. A cylindrical ZrO_2 was used for thermal insulator. Mo electrodes were put at both ends of the heater to connect with anvils electrically. The sample capsule was electrically insulated from the heater using a MgO sleeve and two lids at both ends of the sleeve. All ceramics of the cell assemblies were heated at 1000 $^{\circ}\text{C}$ for >3 h just

before assembling them. Sample temperatures were monitored at the surface of the metal capsules using a W97%Re3%-W75%Re25% thermocouple without its pressure correction to the emf. Pressure calibration at a high temperature of 1600 °C was conducted using the forsterite-wadslevite (Morishima et al. 1994) wadsleyite-ringwoodite (Inoue et al. 2006) transitions in Mg₂SiO₄ and the akimotoite-bridgmanite transition (Chanyshev et al., 2022). We assumed that pressure values at the target temperatures (800–900 °C) were the same as those calibrated at 1600 °C although sample pressure may be changed by degrees of thermal pressure and material softening around the samples, which may change with temperatures (Ishii et al. 2022a). Our previous studies examined pressure generation at high temperatures in the quench method, in which pressures at 1400–1800 °C are consistent but change by 0.5-1 GPa at 2000-2200 °C (Ishii et al. 2011; 2012; 2019b). If such a pressure change also happens at lower temperatures, sample pressures in this study might also change by 0.5-1

In the water partitioning experiments for wadsleyite and ringwoodite, the samples were annealed at 14–16 GPa and 800 $^{\circ}$ C and 21 GPa and 800–900 $^{\circ}$ C, respectively, for 24–28 h. The phase-equilibrium experiments using hydrous wadsleyite and ringwoodite were conducted at 12 GPa and 800 $^{\circ}$ C for 24 h and 20 GPa and 800 $^{\circ}$ C for 20 h, respectively. A cell assembly was first compressed to a desired press load at room temperature for 3–4 h and then gradually heated to a target temperature at a rate of 100 $^{\circ}$ C/min. The target temperature was kept for the desired duration, and then the assembly was immediately quenched by shutting off the electric power supply of the heater. The quenched assembly was recovered slowly to the ambient pressure for 12–15 h.

2.4. Analyses of run products

All analyses below were performed with analytical tools installed at IPM. Sample capsules recovered from high-pressure experiments were mounted in epoxy resin and were polished for phase identification by XRD. XRD analysis was performed using a micro-focus X-ray diffractometer (Rigaku RAPID II) with an imaging plate using CuK α radiation operated at 40 kV and 30 mA. Textures of recovered samples were observed using a field-emission scanning electron microscope (JEOL JSM7001F) equipped with a back-scattered detector.

Water contents of the starting materials and recovered samples of wadsleyite and ringwoodite were measured by unpolarized Fourier transformation infrared spectroscopy (FTIR) using a Jasco FTIR-6200 equipped with an IRT-7000 infrared microscope. The samples were double-polished to 28–206 μm thick for the FTIR measurement. The water contents after the partitioning experiment were measured at locations close to the hydrous silicate matrix with the distance of 20–50 μm (Fig. 1). Water contents in these samples were estimated by integrating OH-related peaks after baseline subtraction (see examples in Figures S1 and S2) as below:

$$C_{H2O} = 10^6 imes \int rac{3A(v)M_{H_2O}}{arepsilon au
ho} dv$$

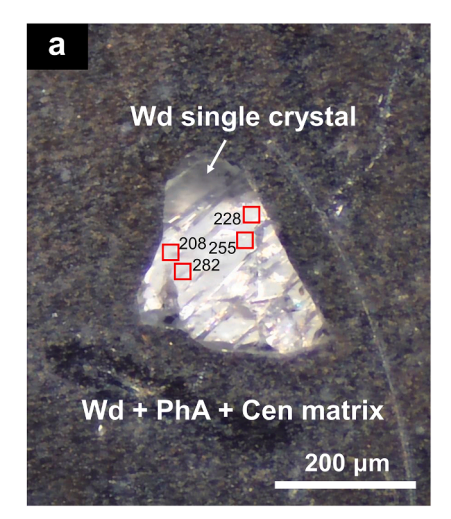
where C_{H2O} is the H_2O content in ppm wt., and $A(\upsilon)$ is the infrared absorption at wavenumber υ (cm $^{-1}$). The molar mass of water (M_{H2O}) is $18.02~g\cdot mol^{-1}$. ε , τ , and ρ are infrared absorption coefficient (69,000 $\pm 5000~L\cdot mol^{-1}\cdot cm^{-2}$ for wadsleyite and $118,500\pm 7000~L\cdot mol^{-1}\cdot cm^{-2}$ for ringwoodite (Bolfan-Casanova et al., 2018)), sample thickness (cm) and density (3450 g·L $^{-1}$ for wadsleyite (Jacobsen et al., 2005) and 3650 g·L $^{-1}$ for ringwoodite (Jacobsen et al., 2004)), respectively. Note that Deon et al. (2010) and Koch-Müller and Rhede (2010) reported ε of 73,000 and 100,000 L·mol $^{-1}\cdot cm^{-2}$ for wadsleyite and ringwoodite, respectively, providing by 5 % and 16 % systematically lower and higher water contents.

3. Results and discussion

Tables 1, S1 and S2 summarize conditions of high-pressure experiments and their results. Figs. 2 and 3 show micro-FTIR spectra of the starting and recovered wadsleyite single crystals and ringwoodite aggregates, respectively, at ambient conditions. XRD patterns of recovered samples were shown in Figures S3 and S4.

3.1. Water partitioning experiments of wadsleyite

We conducted three experiments at 14 and 16 GPa at 800 °C (Table 1). XRD patterns of recovered matrix parts identified wadsleyite, clinoenstatite, and hydrous phase A (Figure S3). Three peaks of 3206, 3323, and 3352 cm⁻¹ were observed in most FTIR spectra (Fig. 2). Positions of these peaks showed no significant change in their profiles before/after experiments, but their intensities were slightly changed, suggesting changes in their water contents. The water content of wadsleyite after annealing was estimated to be 222(13) ppm at 14 GPa and 214(28) ppm at 16 GPa in experiments using the starting wadsleyite



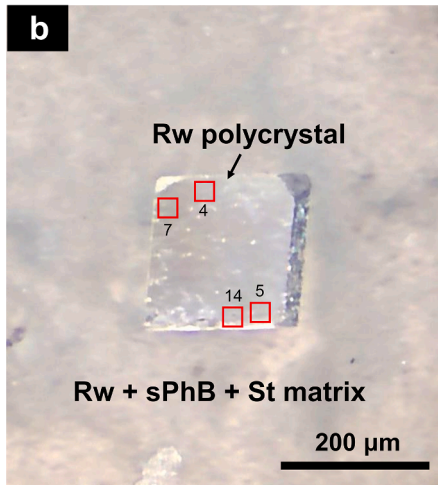


Fig. 1. Representative photographs of cross-sections of recovered samples. (a) Wadsleyite (Wd) in Wd + clinoenstatite (Cen) + hydrous phase A (PhA) matrix synthesized at 16 GPa and 800 $^{\circ}$ C using nearly dry Wd (1k3860). (b) Ringwoodite (Rw) in Rw + stishovite (St) + superhydrous phase B (sPhB) matrix synthesized at 21 GPa and 800 $^{\circ}$ C using dry Rw (1k3921). Red squares and numbers are regions (25 \times 25 μ m) for the FTIR measurements and estimated water content in ppm wt. (Table S1).

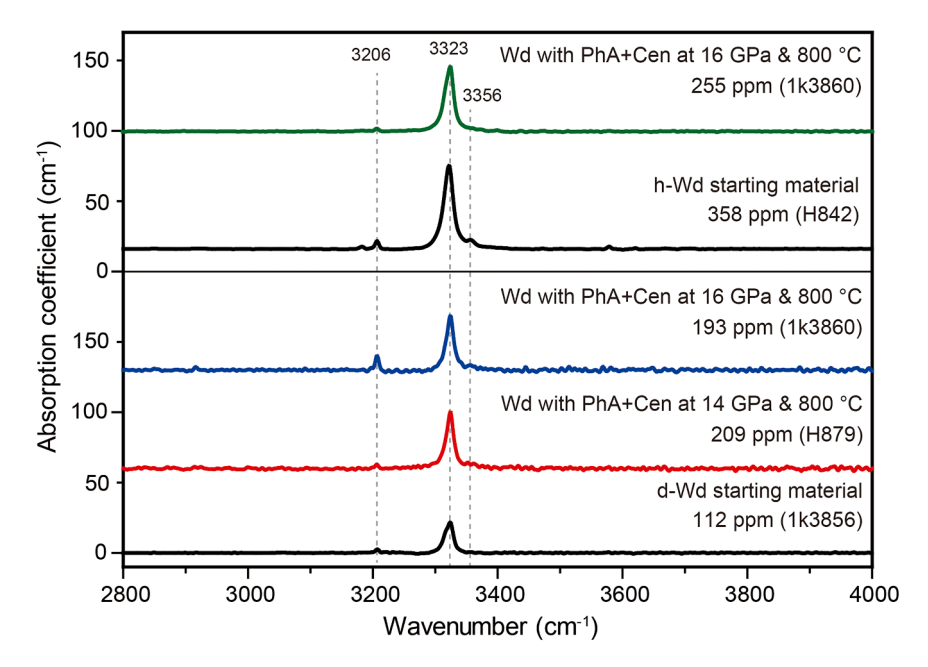


Fig. 2. Representative unpolarized FTIR spectra of wadsleyite (Wd) single crystals coexisting with hydrous phase A (PhA) and clinoenstatite (Cen) synthesized at 16 GPa and 800 °C. d-Wd, nearly dry wadsleyite; h-Wd, slightly hydrated wadsleyite.

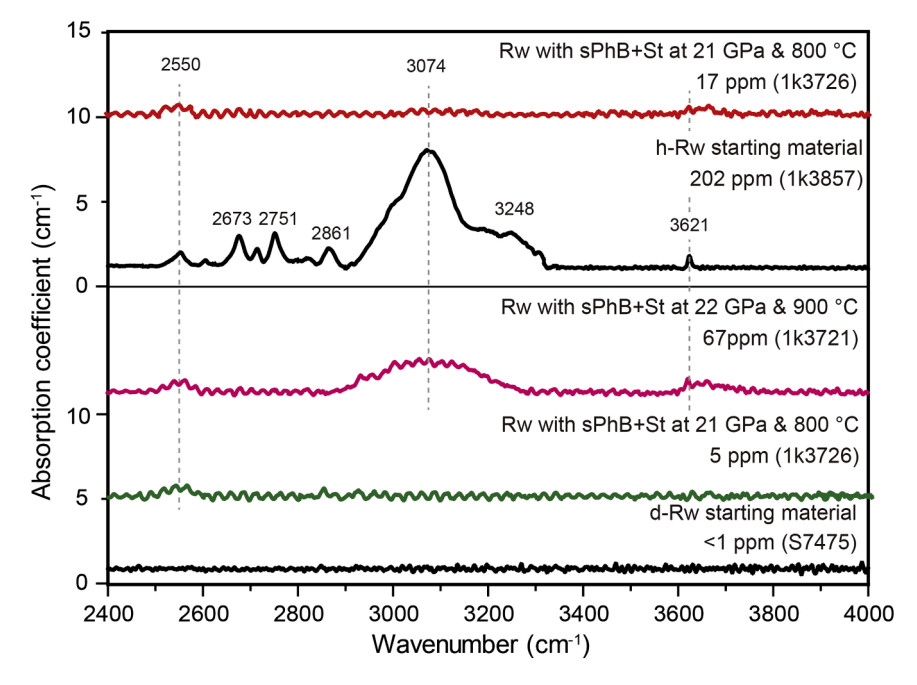


Fig. 3. Representative unpolarized FTIR spectra of ringwoodite (Rw) polycrystal aggregates coexisting with superhydrous phase B and stishovite (St) synthesized at 21 GPa and 800–900 °C. d-Rw, dry ringwoodite; h-Rw, slightly hydrated ringwoodite.

with 361(13) ppm water (Table 1, Fig. 4), showing decreases in the water content >100 ppm from the starting content. We also conducted an experiment at 16 GPa using the starting wadsleyite with 121(12) ppm water. The recovered wadsleyite had 244(28) ppm water, showing an increase in water >100 ppm from the starting content (Table 1, Fig. 4). As a result, water contents of wadsleyite were converged to \sim 200 ppm, suggesting equilibrium in hydrogen between the wadsleyite single crystals and hydrous matrix part during our experiments. These results are consistent with those of Ishii and Ohtani (2021) at a lower pressure of 12 GPa and temperatures of 800–900 °C. Note that Ishii and Ohtani (2021) confirmed only decrease in water content from that of the starting wadsleyite. Our study confirmed validity of their data by

observing both of the increase and decrease in water content using wadsleyite starting materials with different water contents. Demouchy et al. (2005) conducted an experiment at 15 GPa and 900 °C, showing a mineral assemblage of wadsleyite + melt + fluid and 2.23 wt.% water in wadsleyite. They observed not hydrous phase but silicate melt + excess fluid instead, indicating that the system is oversaturated in water. This would be the reason of the high-water content in wadsleyite at their condition. Additionally, the sample temperatures of these two studies may be different due to some uncertainty of temperature measurements by thermocouple. Thus, there seems no pressure dependence on water content of wadsleyite coexisting with hydrous phase A.

Water content of coexisting clinoenstatite could be lower than the

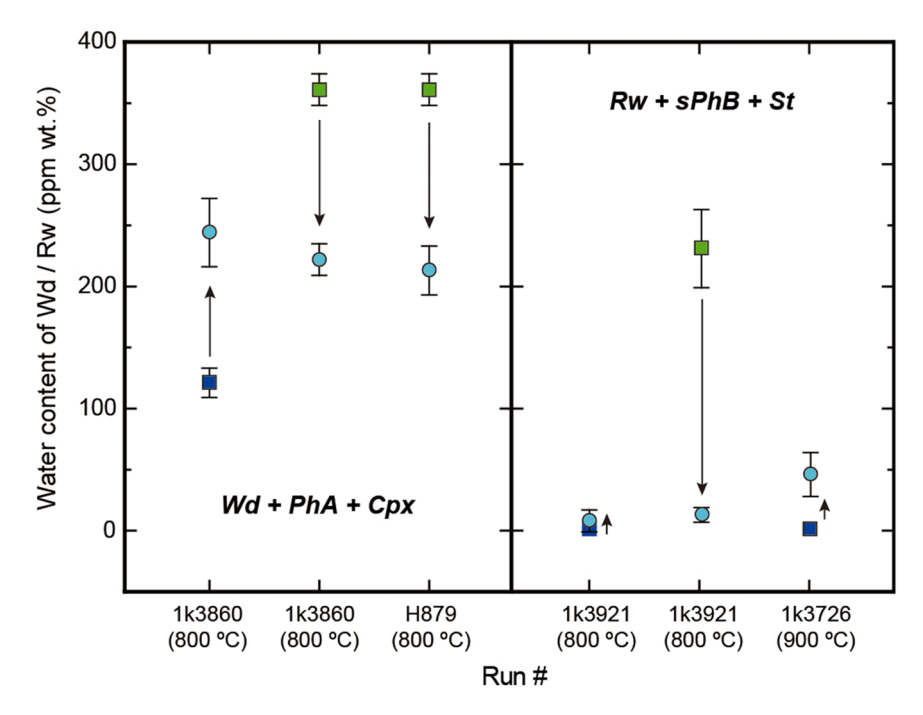


Fig. 4. Change of water contents of wadsleyite (Wd) and ringwoodite (Rw) coexisting with hydrous phase A (PhA) plus clinopyroxene (Cpx) and superhydrous phase B (sPhB) plus stishovite (St) before/after annealing. Arrows indicate the changes from water contents in starting materials (solid squares) to those after annealing (solid circles).

coexisting wadsleyite. Bolfan-Casanova et al. (2000) investigated water partitioning between $\rm Mg_2SiO_4$ wadsleyite and $\rm MgSiO_3$ clinoenstatite, showing a partitioning coefficient between wadsleyite and clinoenstatite coexisting with hydrous melt is $\sim\!3.8$ at 15 GPa and 1300 °C. When we apply this value to the present conditions, water contents of clinoenstatite in this study were estimated to be 56–64 ppm. Considered coexistence of hydrous phase A in the present conditions, water content can be even lower.

3.2. Water partitioning experiments of ringwoodite

Experiments at 21 GPa and 800-900 °C were carried out to examine water content of ringwoodite (Table 1). XRD patterns of the recovered matrix parts (9Fo+1[2Br+Qz]) showed a mineral assemblage of ringwoodite, stishovite, and superhydrous phase B (Figure S3). Several OHbands at \sim 2550, 3074, and 3621 cm⁻¹ were observed in the starting material of slightly hydrated ringwoodite and ringwoodite after annealing (Fig. 3). The starting polycrystalline ringwoodite with water <1 ppm was hydrated to 8(9) ppm at 800 °C and to 46(18) ppm at 900 °C, showing a slight positive temperature dependence (Table 1). When we used ringwoodite aggregate with 231(32) ppm for the experiment at 21 GPa and 800 $^{\circ}$ C, significant intensity decrease was observed in FTIR spectra of the ringwoodite aggregate, resulting in 13(6) ppm water in ringwoodite after annealing (Table 1, Fig. 4). These results suggest that the experiments at 800 °C were equilibrium in hydrogen between ringwoodite aggregate and hydrous matrix part. Although no reversal experiment was conducted at 900 $^{\circ}\text{C},$ a higher temperature should reach equilibrium more rapidly.

Water content of coexisting stishovite could be nearly dry when considering temperature dependence of water solubility of stishovite. Recent studies showed water contents in stishovite with hydrous melt linearly decrease with decreasing temperature from $1700\,^{\circ}\text{C}$ to $1200\,^{\circ}\text{C}$, resulting in nearly dry stishovite at $1200\,^{\circ}\text{C}$ (Bolfan-Casanova et al., 2000; Pawley et al., 1993; Purevjav et al. 2024). Considering the lower temperature in this study (800–900 $^{\circ}\text{C}$) and coexistence with superhydrous phase B, stishovite in this study could also be nearly dry.

3.3. Phase-equilibrium experiments with hydrous wadsleyite and ringwoodite

We conducted one experiment using hydrous wadsleyite with 2 wt.% water at 12 GPa and 800 °C. The recovered sample consisted of wadsleyite with fine grains (<1 µm) of clinoenstatite and hydrous phase A, implying hydrous wadsleyite is not stable and decomposed to hydrous phase A and clinoenstatite (Fig. 5a and b, Figure S4). We also conducted one experiment using hydrous ringwoodite with 1.6 wt.% water at 20 GPa and 800 °C. The recovered sample consisted of ringwoodite with fine grains of stishovite and superhydrous phase B (Fig. 5c and d, Figure S4). This experiment also suggests hydrous ringwoodite is not stable and decomposed to superhydrous phase B and stishovite. This study confirmed stability of hydrous phase A and superhydrous phase B coexisting with wadsleyite and ringwoodite, respectively, based on formation of hydrous minerals by the decompositions of highly hydrated wadsleyite and ringwoodite. These results further support limited water contents of wadsleyite and ringwoodite coexisting with hydrous phase A and superhydrous phase B, respectively. We note that these starting wadsleyite and ringwoodite had no additional phases before annealing (Figure S5), clearly showing appearance of the hydrous phases by decompositions of wadsleyite and ringwoodite.

Previous studies indicate water-content dependence on the stability of hydrous phases in the MgO-SiO₂-H₂O systems. When comparing results at an Mg/Si ratio of 2.0, the present study in the system of MgO-SiO₂-H₂O (2.5 wt.% water) found that superhydrous phase B is stable at 20–21 GPa and 800–900 °C. On the other hand, hydrous phase D coexists in the system with higher water contents of 11 wt.%H₂O (Ohtani et al. 2000). This suggests that the stability of hydrous minerals largely depends on the water content in the system.

We also compare the stability of hydrous minerals at different Mg/Si ratios. Irifune et al. (1998) reported that hydrous phase A is stable up to 17 GPa and 800 °C in the serpentine system (Mg/Si=1.5 and 13 wt.% water), in which no forsterite and its high-pressure polymorphs coexist. At 16–17 GPa, hydrous phase D coexists with hydrous phase A, although in the system of MgO-SiO₂-H₂O (Mg/Si=2.0–2.2 and 2–4.9 wt.% water) the present study and Ishii and Ohtani (2021) showed no hydrous phase

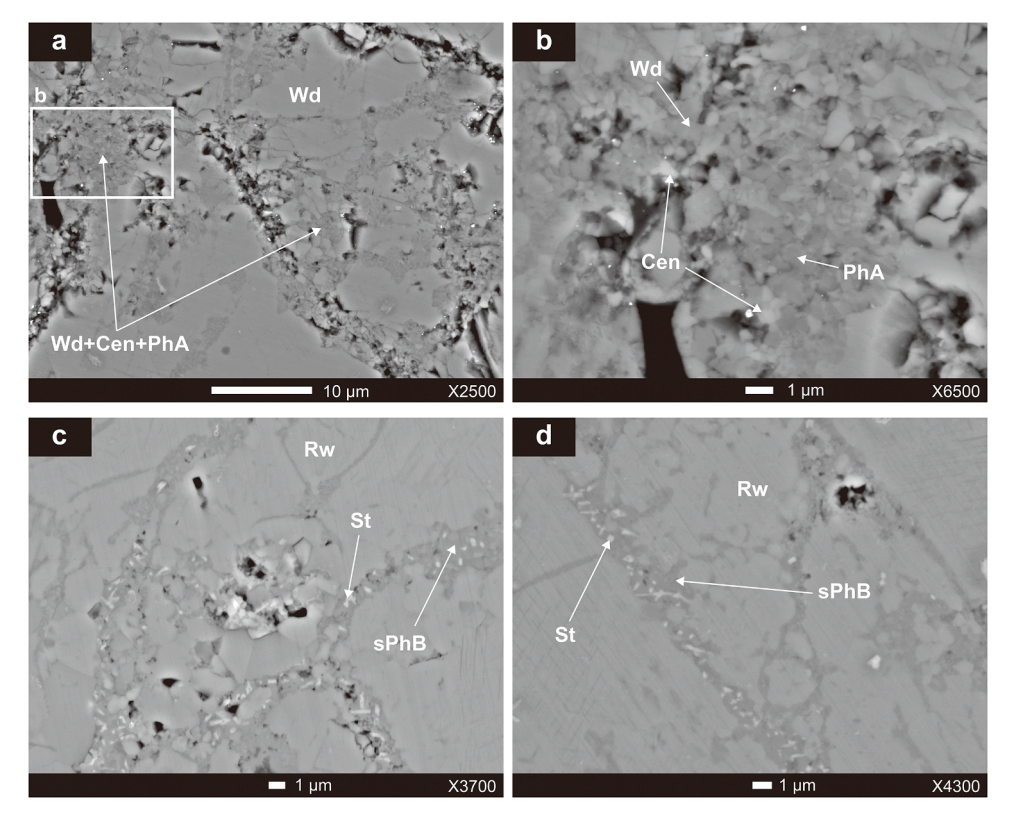


Fig. 5. Back-scattered electron images of recovered samples using highly-hydrated wadsleyite (Wd) and ringwoodite (Rw) as starting materials. (a,b) 12 GPa and 800 °C. (c,d) 20 GPa and 800 °C. PhA: hydrous phase A, sPhB: superhydrous phase B, Cen: clinoenstatite, St: stishovite.

D at 12-16 GPa and 800-900 °C. Thermodynamic models of phase-relations based on high-pressure experiments (Mg/Si=1.4-2.0 and H₂O content=3.66-15 wt.%) and thermodynamic data can be used to predict phase relations in the MgO-SiO2-H2O system under a water-undersaturated condition at the pressure-temperature conditions of this study (Komabayashi et al. 2005; Komabayashi and Omori, 2006). These models predict that hydrous phase E or superhydrous phase B are mainly stable at 14-16 GPa and 800-900 °C and hydrous phase A is stable below 800 $^{\circ}$ C. The subtle differences from the present study may be due to extrapolation of phase stability data from higher temperature (>1000 $^{\circ}\text{C}$). Because Mg/Si ratios in the above studies are not consistent (1.4-2.0), slightly different mineral assemblages were formed. This might also change the stability of hydrous minerals. Nevertheless, these observations imply that the stability of hydrous minerals largely depends on water content in the system. Results in the present study and previous studies indicate that hydrous phase A and superhydrous phase B could be primary water carriers in the transition zone under water undersaturated conditions. Note that this study provided only limited data of phase-relations, and future studies conducting at detailed pressure-temperature-composition conditions, especially water-undersaturated systems, are necessary to examine the stability of hydrous phases.

3.4. Water contents of wadsleyite and ringwoodite with increasing temperature

Fig. 6a shows water contents of ringwoodite with increasing temperature using our results together with the previous data above 1200 °C under water-saturated conditions. There seems to be a small temperature dependence up to 900 °C. This suggests the slight reaction of superhydrous phase B + stishovite to hydrous ringwoodite with temperature. Based on the phase rule, the stability region of ringwoodite + superhydrous phase B + stishovite is divariant in the MgO-SiO₂-H₂O system, indicating continuous compositional change with temperature

at a constant pressure in the stability field. Therefore, the water content of ringwoodite can increase rapidly and continuously up to the temperature where the hydrous phase disappears (Fig. 6b). The phase relation of the above reaction is given in Fig. 6c. In fact, Komabayashi and Omori (2006) reported high-water contents of ringwoodite (0.94–1.31 wt.%) coexisting with superhydrous phase B and stishovite synthesized at 20.5-21.5 GPa and 1100-1200 °C (Mg/Si=1.4 and 3.66 wt%H2O) based on mass deficit determined by electron microprobe analysis (EPMA) (Fig. 6a). On the other hand, Ohtani et al. (2000) showed water contents of ringwoodite are 1.2-2.2 wt.% at 20-23 GPa and 880 $^{\circ}\text{C}$ also by EPMA mass deficit. This discrepancy with the present study confirms that a more precise analysis as shown in this study is essential to precisely discuss water contents of NAMs as reported in previous studies (e.g. Bolfan-Casanova et al. 2018; Fei and Katsura, 2020). Note that the degree of hydration of ringwoodite depends on bulk water content.

A similar feature should be able to be seen in wadsleyite coexisting with hydrous phase A. Water content in wadsleyite coexisting with hydrous phase A seems no change up to 900 °C at 12–16 GPa (this study; Ishii and Ohtani, 2021). Thus, the rapid increase of water content of wadsleyite can happen by the reaction of hydrous phase A + clinoenstatite to hydrous wadsleyite up to the disappearance temperature of hydrous phase A. Note that hydrous phase A changes to other hydrous phases at a higher temperature depending on pressure (e.g. hydrous phase E at 15.5 GPa and 1000 °C and superhydrous phase B at 18.5 GPa and 1100 °C, Komabayashi and Omori, 2006). Komabayashi and Omori (2006) reported water contents of 1.78–2.71 wt.% at 15.5–18.5 GPa and 1000–1100 °C in wadsleyite coexisting with hydrous phase E or superhydrous phase B + stishovite based on Mg/Si ratio determined by EPMA.

3.5. Water content of forsterite and its high-pressure polymorphs, and bridgmanite with increasing pressure

Fig. 7 summarizes water contents of forsterite, wadsleyite,

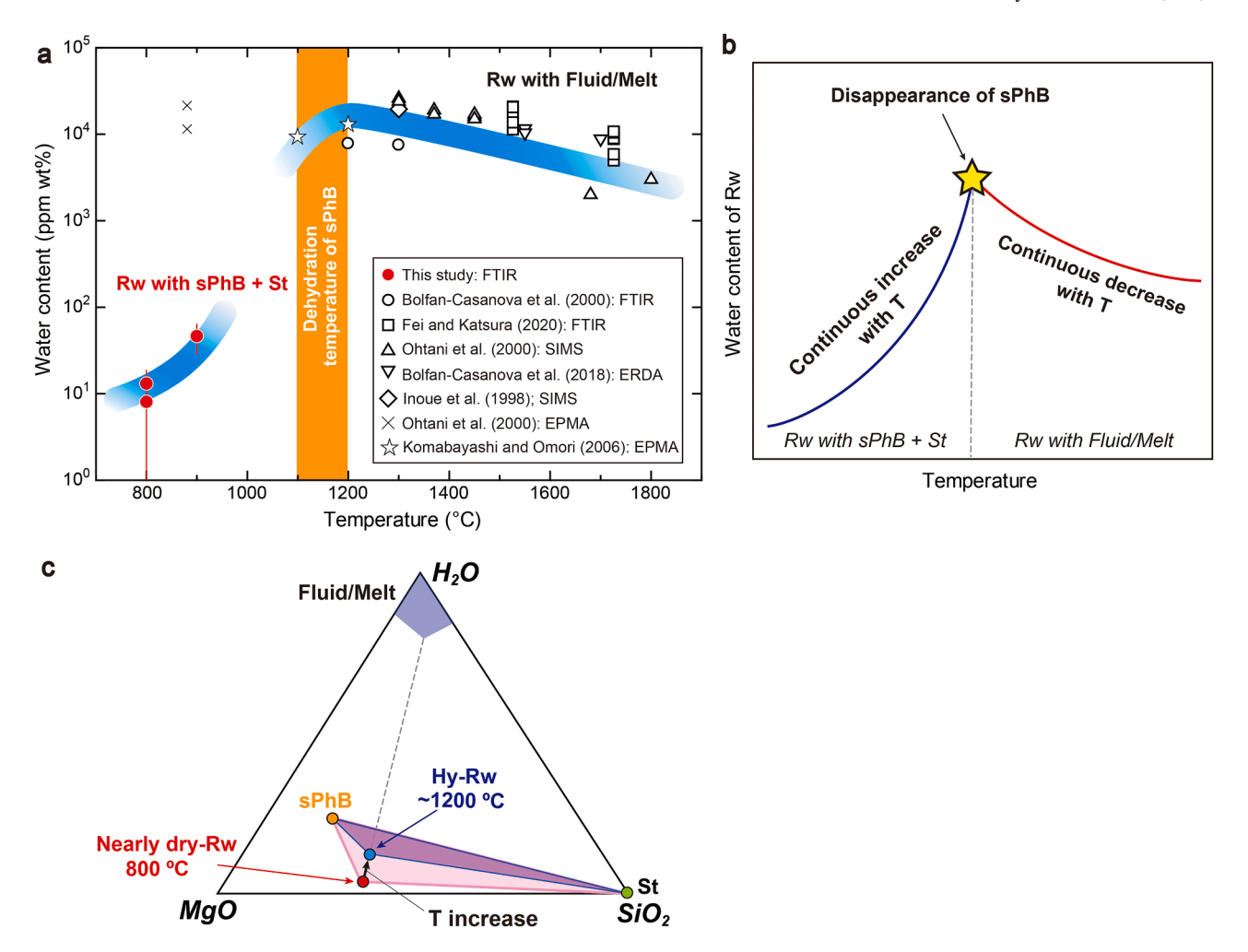


Fig. 6. (a) The water content in ringwoodite (Rw) with increasing temperature. Data of ringwoodite coexisting with fluid/melt (open circles, diamonds, triangles, inverted triangles, and squares) were taken from Bolfan-Casanova et al. (2000, 2018), Fei and Katsura (2020), Inoue et al. (1998), and Ohtani et al. (2000). Our data of ringwoodite coexisting with hydrous phases plotted together with data from Ohtani et al. (2000) (crosses) and Komabayashi and Omori (2006) (open stars). The approximate dehydration temperature was taken from Ohtani et al. (2001). FTIR: Fourier transformation infrared spectroscopy, SIMS: Secondary-ion mass spectrometry, ERDA: elastic recoil detection analysis, EPMA: electron microprobe analysis, sPhB: superhydrous phase B. (b) A thermodynamic interpretation of water content change of ringwoodite with temperature. (c) A schematic phase relation of the MgO-SiO₂-H₂O system at 800 and ~1200 °C at ~20 GPa.

ringwoodite, and bridgmanite coexisting with hydrous phases under cold slab temperatures and water-undersaturated conditions determined in this study and previous studies (Bolfan-Casanova et al., 2003; Ishii and Ohtani, 2021; Ishii et al. 2022b). Combined the present results and those by Ishii and Ohtani (2021), there seems no pressure dependence in water partitioning in forsterite/wadsleyite and hydrous phase A. Although the data of ringwoodite is limited only at 21 GPa, it is likely that there is limited pressure dependence based on the results of forsterite and wadsleyite. Bridgmanite is also nearly dry when coexisting with superhydrous phase B/hydrous phase D and/or hydrous phase δ -H solid solution at least up to 28 GPa (Bolfan-Casanova et al. 2003; Ishii et al. 2022b). Our recent study also demonstrated that stishovite is nearly dry when coexisting with hydrous phase δ (Ishii et al. 2024). These results suggest that the strong water partitioning to hydrous phases is a common phenomenon among mantle minerals.

3.6. Implications for structure and dynamics of subducting slab

Here we discuss a detailed structure of a wet subducting slab (Fig. 8). Our results suggest that olivine and its high-pressure polymorphs are dry or nearly dry when they coexist with hydrous minerals along cold slab core temperatures (500–900 °C) (Kirby et al. 1996). This implies that the dry transformation of olivine can be applied even in wet subducting

slabs, resulting in the metastable olivine wedge (Jiang et al., 2008; Kawakatsu and Yoshioka, 2011) and the deep-focus earthquakes (Kirby et al., 1991). Slab deformation observed around the 660-km discontinuity requires to lower viscosity of the slab core. Thus, grain size reduction in the slab core due to the dry olivine transformation to ringwoodite is a plausible explanation for slab large deformation to create slab stagnation around the 660-km discontinuity (Mohiuddin et al. 2020). When hydrous minerals experience near or at disappearance temperatures of the hydrous minerals outside the slab core, hydrolytic weakening of olivine polymorphs occurs and can help cause slab deformation and stagnation together with grain-size reduction at the slab core. Thus, there may be a rheological boundary near the disappearance temperature of the hydrous phases in the slabs. Relatively low thermal conductivities of hydrated NAMs and hydrous minerals can efficiently preserve the mineralogical structure (nearly dry NAMs and hydrous minerals) in the slab core, supporting slab dynamics and deep-focus earthquakes controlled by dry olivine transformations (Hsieh et al. 2020, 2022; Marzotto et al. 2020;).

Rheological properties of hydrous minerals are not clear yet. Rosa et al. (2013) determined strength of hydrous phase D, suggesting that hydrous phase D has relatively low strength compared with phases in peridotite at the top lower mantle. If this is also the case for other hydrous minerals such as superhydrous phase B, such a low strength

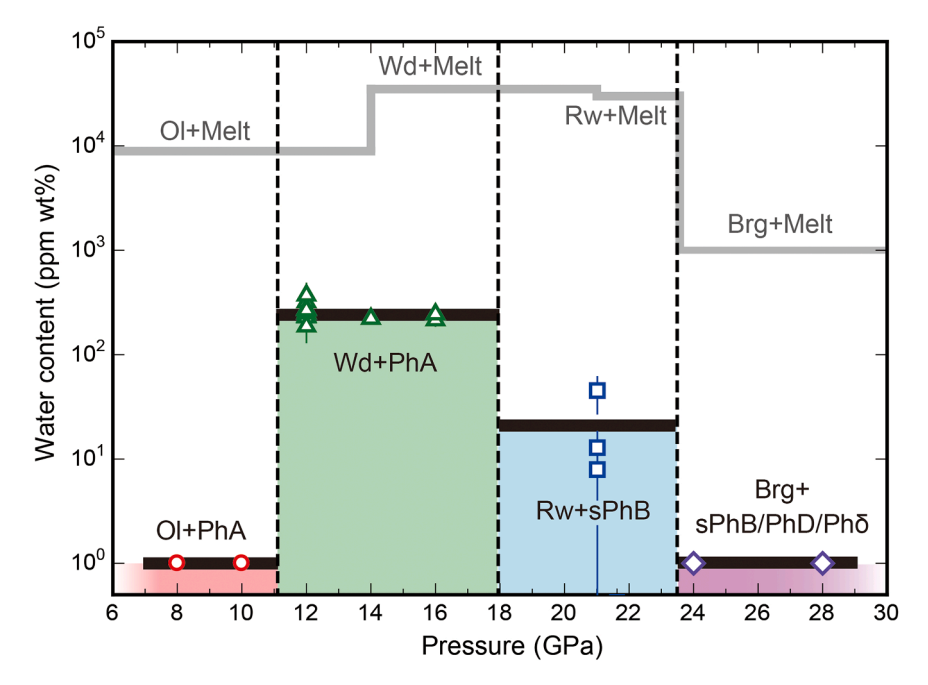


Fig. 7. Water contents of major mantle minerals coexisting with hydrous phases. Water contents of olivine/wadsleyite + hydrous phase A at 8–12 GPa and 800–900 °C were taken from Ishii and Ohtani (2021). Those of bridgmanite+superhydrous phase B/hydrous phase D/hydrous phase δ were taken from Bolfan-Casanova et al. (2003) and Ishii et al. (2022b). The dashed lines are approximated transition pressures of olivine-wadsleyite (800 °C) and wadsleyite-ringwoodite (900 °C), and ringwoodite-bridgmanite + periclase (1000 °C) transitions at 800 °C and 900 °C (Katsura et al. 2004; Inoue et al. 2006; Chanyshev et al. 2022). Ol, olivine; PhA, hydrous phase A;; Wd, wadsleyite; Rw, ringwoodite; sPhB, superhydrous phase B; PhD, hydrous phase D; Phδ, hydrous phase δ. Additional phases such as clinoenstatite and stishovite in Ol/Wd and Rw regions, respectively, are ignored in this diagram. Gray lines are water solubility of major mantle minerals coexisting with hydrous melt (Fu et al. 2019; Inoue et al. 1995; Kohlsted et al. 1996; Smyth et al., 2006).

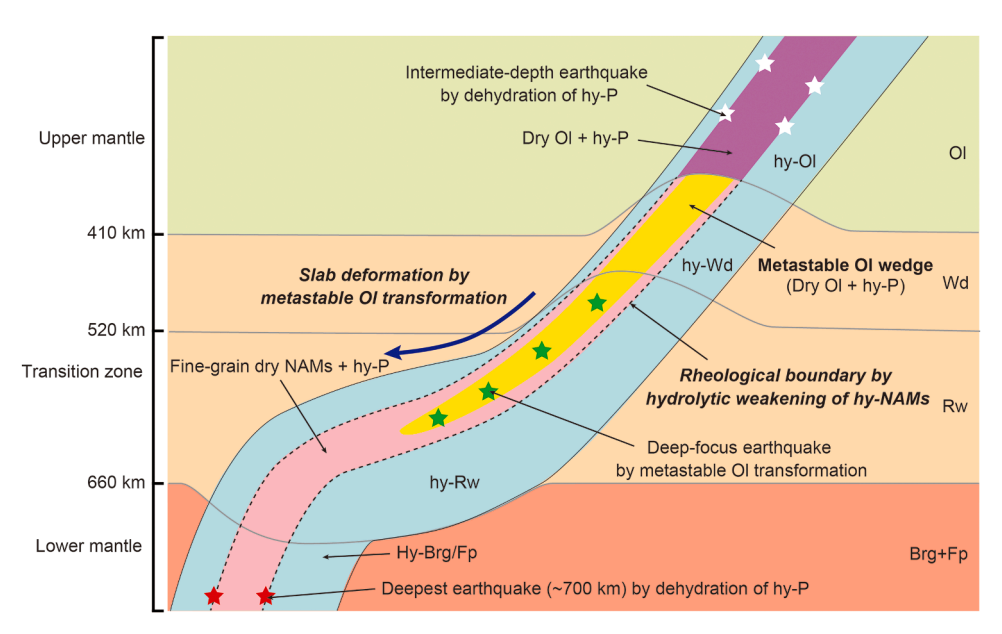


Fig. 8. Structure and dynamics of a wet subducting slab. Dry olivine (Ol) + hydrous phase (hy-P) in a cold slab core (purple) becomes metastable Ol + hy-P (yellow) below the 410-km discontinuity. Metastable Ol transforms to fine-grained dry wadsleyite (Wd), ringwoodite (Rw), or bridgmanite (Brg) + ferropericlase (Fp) with depth (pink). The solid black line indicates a boundary between the slab and mantle. The black dashed lines show a possible rheological boundary formed by hydrolytic weakening of hydrated nominally anhydrous minerals (NAMs) (blue).

property of hydrous minerals can affect slab dynamics. To consider rheology of a hydrous phase-bearing slab, texture of such weak phases is an important issue: homogeneous distribution or localization of the phases (Rosa et al. 2013; 2015). Hydrous phases near the Earth's surface are likely formed by reactions between anhydrous minerals and sea water preserved along fluid pathways such as bending fault making band texture of hydrous minerals (Peacock, 2001; Cai et al. 2018). Water

supply into slabs before subduction by upwelling plumes including Petit spot volcanism may also form a largely-hydrated region in the slabs (Seno and Yamanaka, 1996; Hirano et al. 2006). Hydrous phases such as serpentine formed by these processes can transform to dense hydrous phases such as hydrous phase A, superhydrous phase B, and hydrous phase D with keeping such a band texture. If this is the main case, such a texture favors strain localization along shear band that contains

rheologically weak hydrous phases (Hilairet et al., 2007; Rosa et al., 2013; Seaman et al., 2013). This process may enhance slab deformation to produce stagnant slabs (Fukao and Obayashi, 2013).

It has been considered that water is first incorporated into NAMs such as olivine and its high-pressure polymorphs and the remained water forms hydrous minerals (e.g. Faccenda, 2014). However, our results revealed that hydrous minerals are formed to accommodate water at relatively low temperatures corresponding to a cold slab core, remaining NAMs dry. Thus, most water is trapped in dense hydrous phases and the major constituents such as olivine, wadsleyite, and ringwoodite in wet slabs are dry. Dense hydrous phases can be the main water carrier also in the lower mantle after ringwoodite transforms to bridgmanite assemblage because lower-mantle minerals such as bridgmanite and ferropericlase can accommodate very limited water (Keppler and Bolfan-Casanova, 2006; Fu et al. 2019). Due to temperature increase of harzburgitic/peridotitic layer of the slabs by the high-temperature lower mantle, dense hydrous magnesium silicates will finally release water because of their limited thermal stability below the average mantle temperature (e.g. Ghosh and Schmidt, 2014; Nishi et al. 2015). The released water will be captured by a basaltic layer, which is a silica-enriched rock consisting of silica polymorphs such as stishovite and CaCl2-type phase, bridgmanite, davemaoite, Al-rich phases of calcium ferrite-phase and hexagonal phase (Hirose et al. 2005; Ishii et al. 2019b, 2022c). Reactions of the basaltic layer with water could make hydrous aluminous silica phases (Ishii et al. 2022d; Lin et al. 2020; 2022; Litasov et al. 2007; Tsutsumi et al. 2024) and the main water carrier is changed to them in the basaltic layer.

Deep-focus earthquakes have been observed down to ~700 km depth (e.g. Zhan, 2020). The metastable olivine transformation is one of the possible mechanisms and can partly explain deep-focus earthquakes (Kirby et al. 1996). It is generally considered that dehydration of hydrous minerals causes embrittlement of rocks, which is an origin of intermediate-depth earthquakes. Dehydration of hydrous minerals (Omori et al. 2004; Shirey et al. 2021) has also been invoked as a possible mechanism to trigger deep-forcus earthquakes. Note that at temperatures below the dehydration of hydrous minerals to wadsleyite or ringwoodite (~1200 °C), the water content of the subducting slab mantle must be more than water solubility of NAMs when considering dehydration embrittlement, because as we show here in the water under-saturated slabs, dehydrated water is absorbed to the NAMs and dehydration embrittlement is less likely to occur in slabs subducting in the transition zone. At higher pressures, water solubilities of bridgmanite and ferropericlase are relatively low <0.1 wt.% (e.g. Bolfan--Casanova et al. 2003; Fu et al. 2019). Therefore, dehydration of hydrous minerals such as superhydrous phase B and hydrous phase D in the stability field of bridgmanite may provide a reasonable explanation for the deepest earthquakes around 700 km depth (Komabayashi et al. 2004; Omori et al. 2004; Shirey et al., 2021; Zahradnik et al., 2017) (Fig. 8).

4. Conclusion

We have conducted water partitioning experiments between wad-sleyite or ringwoodite and hydrous phases down to transition zone conditions. We found that nearly dry wadsleyite and ringwoodite coexist with hydrous phase A and superhydrous phase B at 14–16 GPa and 21 GPa at least up to 900 °C, respectively. These results suggest main water carriers in a cold slab core down to the transition zone could be these dense hydrous magnesium silicates. These results indicate that dry olivine coexisting with hydrous phase A transforms to nearly dry wadsleyite or ringwoodite and hydrous phase A or superhydrous phase B, respectively. Thus, grain-size reduction by dry olivine transformations in a cold slab core could control rheology of a subducting slab and form slab stagnation and deep-focus earthquakes around 450–660 km depths. Combined with previous studies of water partitioning between NAMs and hydrous phases (Bolfan-Casanova et al., 2003; Ishii and Ohtani,

2021; Ishii et al. 2022b), main water carriers at least down to uppermost lower mantle depths are hydrous phases. Dehydration of hydrous phases could cause the deepest earthquakes happened around 700 km depths due to limited water solubility of major lower mantle minerals of bridgmanite and ferropericlase. The present phase relations of hydrous phases coexisting with NAMs at systems with relatively low water contents (1.6–2.5 wt.%) are significantly different from those with high water contents (11 wt.%) (e.g., Ohtani et al. 2001). Future study of the detailed phase relations at such water undersaturated conditions will provide more detailed view of water distribution and water circulation in the mantle.

CRediT authorship contribution statement

Takayuki Ishii: Writing – original draft, Visualization, Validation, Supervision, Project administration, Methodology, Investigation, Funding acquisition, Formal analysis, Data curation, Conceptualization. **Jintao Zhu:** Writing – review & editing, Investigation, Formal analysis. **Eiji Ohtani:** Writing – review & editing, Funding acquisition, Conceptualization.

Declaration of competing interest

The authors declare that they have no known competing financial interests or personal relationships that could have appeared to influence the work reported in this paper.

Acknowledgement

We thank R. Njul for preparation of thin-section samples. This work was supported by the Grants-in-Aid of the German Research Foundation (no. IS350/1–1 for T.I.) and the Kakenhi Grant from Japan Society for the Promotion of Science (20H00187 and 24K00722 for E.O. and 23K19067 and 24K00735 for T.I.). E.O. was also supported by the research award from the Alexander von Humboldt foundation. J.Z. was supported by the Joint Use Program at IPM (Project Number I23-014). We also thank Michael Walter and an anonymous reviewer for their constructive comments.

Supplementary materials

Supplementary material associated with this article can be found, in the online version, at doi:10.1016/j.epsl.2025.119310.

Data availability

Data will be made available on request.

References

Bolfan-Casanova, N., Keppler, H., Rubie, D.C., 2000. Water partitioning between nominally anhydrous minerals in the MgO–SiO₂–H₂O system up to 24 GPa: implications for the distribution of water in the Earth's mantle. Earth. Planet. Sci. Lett. 182 (3–4), 209–221. https://doi.org/10.1016/S0012-821X(00)00244-2.

Bolfan-Casanova, N., Keppler, H., Rubie, D.C., 2003. Water partitioning at 660 km depth and evidence for very low water solubility in magnesium silicate perovskite. Geophys. Res. Lett. 30 (17). https://doi.org/10.1029/2003GL017182.

- Bolfan-Casanova, N., Schiavi, F., Novella, D., Bureau, H., Raepsaet, C., Khodja, H., Demouchy, S., 2018. Examination of water quantification and incorporation in transition zone minerals: wadsleyite, ringwoodite and phase D using ERDA (elastic recoil detection analysis). Front. Earth. Sci. 6, 75. https://doi.org/10.3389/ feart.2018.00075.
- Cai, C., Wiens, D.A., Shen, W., Eimer, M., 2018. Water input into the Mariana subduction zone estimated from ocean-bottom seismic data. Nature 563 (7731), 389–392. https://doi.org/10.1038/s41586-018-0655-4.
- Chanyshev, A., Ishii, T., Bondar, D., Bhat, S., Kim, E.J., Farla, R., et al., 2022. Depressed 660-km discontinuity caused by akimotoite-bridgmanite transition. Nature 601 (7891), 69–73. https://doi.org/10.1038/s41586-021-04157-z.
- Deon, F., Koch-Müller, M., Rhede, D., Gottschalk, M., Wirth, R., Thomas, S.M., 2010. Location and quantification of hydroxyl in wadsleyite: new insights. Am. Mineralog. 95 (2–3), 312–322. https://doi.org/10.2138/am.2010.3267.

- Demouchy, S., Deloule, E., Frost, D.J., Keppler, H., 2005. Pressure and temperature-dependence of water solubility in Fe-free wadsleyite. Am. Mineralog. 90 (7), 1084–1091. https://doi.org/10.2138/am.2005.1751.
- Faccenda, M., 2014. Water in the slab: a trilogy. Tectonophysics. 614, 1–30. https://doi.org/10.1016/j.tecto.2013.12.020.
- Fei, H., Katsura, T., 2020. High water solubility of ringwoodite at mantle transition zone temperature. Earth Planet. Sci. Lett. 531, 115987. https://doi.org/10.1016/j. epsl 2019 115987
- Fukao, Y., Obayashi, M., 2013. Subducted slabs stagnant above, penetrating through, and trapped below the 660 km discontinuity. J. Geophys. Res. 118 (11), 5920–5938. https://doi.org/10.1002/2013JB010466.
- Fu, S., Yang, J., Karato, S.I., Vasiliev, A., Presniakov, M.Y., Gavriliuk, A.G., et al., 2019. Water concentration in single-crystal (Al, Fe)-bearing bridgmanite grown from the hydrous melt: implications for dehydration melting at the topmost lower mantle. Geophys. Res. Lett. 46 (17–18), 10346–10357. https://doi.org/10.1029/ 2019GL084630.
- Green, H.W., Houston, H., 1995. The mechanics of deep earthquakes. Annu. Rev. Earth Planet Sci. 23, 169–214. https://doi.org/10.1146/annurev.ea.23.050195.001125. Volume 23, pp. 169-214.
- Ghosh, S., Schmidt, M.W., 2014. Melting of phase D in the lower mantle and implications for recycling and storage of H₂O in the deep mantle. Geochim. Cosmochim. Acta 145, 72–88. https://doi.org/10.1016/j.gca.2014.06.025.
- Hilairet, N., Reynard, B., Wang, Y., Daniel, I., Merkel, S., Nishiyama, N., Petitgirard, S., 2007. High-pressure creep of serpentine, interseismic deformation, and initiation of subduction. Science 318 (5858), 1910–1913. https://doi.org/10.1126/ science.1148494.
- Hirano, N., Takahashi, E., Yamamoto, J., Abe, N., Ingle, S.P., Kaneoka, I., et al., 2006. Volcanism in response to plate flexure. Science 313 (5792), 1426–1428. https://doi. org/10.1126/science.1128235.
- Hirose, K., Takafuji, N., Sata, N., Ohishi, Y., 2005. Phase transition and density of subducted MORB crust in the lower mantle. Earth. Planet. Sci. Lett. 237 (1–2), 239–251. https://doi.org/10.1016/j.epsl.2005.06.035.
- Hsieh, W.P., Marzotto, E., Ishii, T., Dubrovinsky, L., Aslandukova, A.A., Criniti, G., et al., 2022. Low thermal conductivity of hydrous phase D leads to a self-preservation effect within a subducting slab. J. Geophysic. Res. 127 (6), e2022JB024556. https://doi.org/10.1029/2022JB024556.
- Hsieh, W.P., Ishii, T., Chao, K.H., Tsuchiya, J., Deschamps, F., Ohtani, E., 2020. Spin transition of iron in δ-(Al, Fe) OOH induces thermal anomalies in Earth's lower mantle. Geophys. Res. Lett. 47 (4), e2020GL087036. https://doi.org/10.1029/2020GL087036
- Inoue, T., Weidner, D.J., Northrup, P.A., Parise, J.B., 1998. Elastic properties of hydrous ringwoodite (γ-phase) in Mg₂SiO₄. Earth. Planet. Sci. Lett. 160 (1–2), 107–113. https://doi.org/10.1016/S0012-821X(98)00077-6.
- Inoue, T., Yurimoto, H., Kudoh, Y., 1995. Hydrous modified spinel, Mg_{1.75}SiH_{0.5}O₄: a new water reservoir in the mantle transition region. Geophys. Res. Lett. 22, 117–120.
- Inoue, T., Irifune, T., Higo, Y., Sanehira, T., Sueda, Y., Yamada, A., Shinmei, T., Yamazaki, D., Ando, J., Funakoshi, K., Utsumi, W., 2006. The phase boundary between wadsleyite and ringwoodite in Mg₂SiO₄ determined by in situ X-ray diffraction. Phys. Chem. Mineral. 33, 106–114.
- Irifune, T., 1994. Absence of an aluminous phase in the upper part of the Earth's lower mantle. Nature 370 (6485), 131–133. https://doi.org/10.1038/370131a0.
- Irifune, T., Kubo, N., Isshiki, M., Yamasaki, Y., 1998. Phase transformations in serpentine and transportation of water into the lower mantle. Geophys. Res. Lett. 25 (2), 203–206. https://doi.org/10.1029/97GL03572.
- Irifune, T., Isshiki, M., 1998. Iron partitioning in a pyrolite mantle and the nature of the 410-km seismic discontinuity. Nature 392 (6677), 702–705. https://doi.org/ 10.1038/33663
- Ishii, T., Kojitani, H., Akaogi, M., 2011. Post-spinel transitions in pyrolite and Mg₂SiO₄ and akimotoite-perovskite transition in MgSiO₃: precise comparison by high-pressure high-temperature experiments with multi-sample cell technique. Earth Planet. Sci. Lett. 309 (3–4), 185–197. https://doi.org/10.1016/j.epsl.2011.06.023.
- Ishii, T., Kojitani, H., Akaogi, M., 2012. High-pressure phase transitions and subduction behavior of continental crust at pressure-temperature conditions up to the upper part of the lower mantle. Earth Planet. Sci. Lett. 357, 31–41. https://doi.org/ 10.1016/j.epsl.2012.09.019.
- Ishii, T., Kojitani, H., Akaogi, M., 2018a. Phase relations and mineral chemistry in pyrolitic mantle at 1600–2200 °C under pressures up to the uppermost lower mantle: phase transitions around the 660-km discontinuity and dynamics of upwelling hot plumes. Phys.Earth Planet. Inter. 274, 127–137. https://doi.org/10.1016/j. pepi.2017.10.005.
- Ishii, T., Huang, R., Fei, H., Koemets, I., Liu, Z., Maeda ..., F., Katsura, T., 2018b. Complete agreement of the post-spinel transition with the 660-km seismic discontinuity. Sci. Rep. 8 (1), 6358. https://doi.org/10.1038/s41598-018-24832-y.
- Ishii, T., Huang, R., Myhill, R., Fei, H., Koemets, I., Liu ..., Z., Katsura, T., 2019a. Sharp 660-km discontinuity controlled by extremely narrow binary post-spinel transition. Nat. Geosci. 12 (10), 869–872. https://doi.org/10.1038/s41561-019-0452-1.
- Ishii, T., Kojitani, H., Akaogi, M., 2019b. Phase relations of harzburgite and MORB up to the uppermost lower mantle conditions: precise comparison with pyrolite by multisample cell high-pressure experiments with implication to dynamics of subducted slabs. J. Geophysic. Res. 124 (4), 3491–3507. https://doi.org/10.1029/ 2018JB016749.
- Ishii, T., Ohtani, E., 2021. Dry metastable olivine and slab deformation in a wet subducting slab. Nat. Geosci. 14 (7), 526–530. https://doi.org/10.1038/s41561-021-00756-7.

- Ishii, T., Chanyshev, A., Katsura, T., 2022a. A new approach determining a phase transition boundary strictly following a definition of phase equilibrium: an example of the post-spinel transition in Mg₂SiO₄ system. Minerals 12 (7), 820. https://doi. org/10.3390/min12070820.
- Ishii, T., Ohtani, E., Shatskiy, A., 2022b. Aluminum and hydrogen partitioning between bridgmanite and high-pressure hydrous phases: implications for water storage in the lower mantle. Earth. Planet. Sci. Lett. 583, 117441. https://doi.org/10.1016/j. epsl 2022 117441.
- Ishii, T., Miyajima, N., Criniti, G., Hu, Q., Glazyrin, K., Katsura, T., 2022c. High pressure-temperature phase relations of basaltic crust up to mid-mantle conditions. Earth. Planet. Sci. Lett. 584, 117472. https://doi.org/10.1016/j.epsl.2022.117472.
- Ishii, T., Criniti, G., Ohtani, E., Purevjav, N., Fei, H., Katsura, T., Mao, H.K., 2022d. Superhydrous aluminous silica phases as major water hosts in high-temperature lower mantle. Proceed. Nat. Acad. Sci. 119 (44), e2211243119. https://doi.org/ 10.1073/pnas.2211243119.
- Ishii, T., Criniti, G., Purevjav, N., Katsura, T., Ohtani, E., 2024. Hydrogen partitioning between stishovite and hydrous phase 8: implications for water cycle and distribution in the lower mantle. Prog. Earth. Planet. Sci. 11 (1), 10. https://doi.org/ 10.1186/s40645-024-00615-0.
- Jiang, G., Zhao, D., Zhang, G., 2008. Seismic evidence for a metastable olivine wedge in the subducting Pacific slab under Japan Sea. Earth. Planet. Sci. Lett. 270 (3–4), 300–307. https://doi.org/10.1016/j.epsl.2008.03.037.
- Jacobsen, S.D., Smyth, J.R., Spetzler, H., Holl, C.M., Frost, D.J., 2004. Sound velocities and elastic constants of iron-bearing hydrous ringwoodite. Phys. Earth Planet. Inter. 143, 47–56. https://doi.org/10.1016/j.pepi.2003.07.019.
- Jacobsen, S.D., Demouchy, S., Frost, D.J., Ballaran, T.B., Kung, J., 2005. A systematic study of OH in hydrous wadsleyite from polarized FTIR spectroscopy and singlecrystal X-ray diffraction: oxygen sites for hydrogen storage in Earth's interior. Am. Mineral. 90 (1), 61–70. https://doi.org/10.2138/am.2005.1624.
- Karato, S.I., Jung, H., 2003. Effects of pressure on high-temperature dislocation creep in olivine. Philosophic. Mag. 83 (3), 401–414. https://doi.org/10.1080/ 0141861021000025829.
- Katsura, T., Yamada, H., Nishikawa, O., Song, M., Kubo, A., Shinmei, T., et al., 2004. Olivine-wadsleyite transition in the system (Mg,Fe)₂SiO₄. J. Geophys. Res. 109 (B2). https://doi.org/10.1029/2003JB002438.
- Kawakatsu, H., Yoshioka, S., 2011. Metastable olivine wedge and deep dry cold slab beneath southwest Japan. Earth. Planet. Sci. Lett. 303 (1–2), 1–10. https://doi.org/ 10.1016/j.epsl.2011.01.008.
- Keppler, H., Bolfan-Casanova, N., 2006. Thermodynamics of water solubility and partitioning. Rev. Mineral. Geochem. 62 (1), 193–230. https://doi.org/10.2138/ rmg.2006.62.9.
- Kirby, S.H., Durham, W.B., Stern, L.A., 1991. Mantle phase changes and deep-earthquake faulting in subducting lithosphere. Science 252 (5003), 216–225. https://doi.org/ 10.1126/science.252.5003.216.
- Kirby, S.H., Stein, S., Okal, E.A., Rubie, D.C., 1996. Metastable mantle phase transformations and deep earthquakes in subducting oceanic lithosphere. Rev. Geophys. 34 (2), 261–306. https://doi.org/10.1029/96RG01050.
- Koch-Müller, M., Rhede, D., 2010. IR absorption coefficients for water in nominally anhydrous high-pressure minerals. Am. Mineralog. 95 (5–6), 770–775. https://doi. org/10.2138/am.2010.3358.
- Komabayashi, T., Omori, S., Maruyama, S., 2004. Petrogenetic grid in the system MgO-SiO₂-H₂O up to 30 GPa, 1600°C: applications to hydrous peridotite subducting into the Earth's deep interior. J. Geophys. Res. 109 (B3). https://doi.org/10.1029/2003JB002651.
- Komabayashi, T., Omori, S., Maruyama, S., 2005. Experimental and theoretical study of stability of dense hydrous magnesium silicates in the deep upper mantle. Phys. Earth Plan. Inter. 153 (4), 191–209. https://doi.org/10.1016/j.pepi.2005.07.001.
- Komabayashi, T., Omori, S., 2006. Internally consistent thermodynamic data set for dense hydrous magnesium silicates up to 35 GPa, 1600 C: implications for water circulation in the Earth's deep mantle. Phys. Earth Planet. Inter. 156 (1–2), 89–107. https://doi.org/10.1016/j.pepi.2006.02.002.
- Kohlstedt, D.L., Keppler, H., Rubie, D.C., 1996. Solubility of water in the α, β and γ phases of (Mg,Fe)₂SiO₄. Contribut. Mineral. Petrol. 123, 345–357. https://doi.org/10.1007/s004100050161.
- Kubo, T., Ohtani, E., Kato, T., Shinmei, T., Fujino, K., 1998. Effects of water on the α-β transformation kinetics in San Carlos olivine. Science 281 (5373), 85–87. https://doi.org/10.1126/science.281.5373.85.
- Iidaka, T., Suetsugu, D., 1992. Seismological evidence for metastable olivine inside a subducting slab. Nature 356 (6370), 593–595. https://doi.org/10.1038/356593a0.
- Lin, Y., Hu, Q., Meng, Y., Walter, M., Mao, H.K., 2020. Evidence for the stability of ultrahydrous stishovite in Earth's lower mantle. Proceed. Nat. Acad. Sci. 117 (1), 184–189. https://doi.org/10.1073/pnas.1914295117.
- Lin, Y., Hu, Q., Walter, M.J., Yang, J., Meng, Y., Feng, X., Zhuang, Y., Cohen, R.E., Mao, H.K., 2022. Hydrous SiO₂ in subducted oceanic crust and H₂O transport to the core-mantle boundary. Earth. Planet. Sci. Lett. 594, 117708. https://doi.org/ 10.1016/j.epsl.2022.117708.
- Litasov, K.D., Kagi, H., Shatskiy, A., Ohtani, E., Lakshtanov, D.L., Bass, J.D., Ito, E., 2007. High hydrogen solubility in Al-rich stishovite and water transport in the lower mantle. Earth. Planet. Sci. Lett. 262 (3–4), 620–634. https://doi.org/10.1016/j. epsl.2007.08.015.
- Marzotto, E., Hsieh, W.P., Ishii, T., Chao, K.H., Golabek, G.J., Thielmann, M., Ohtani, E., 2020. Effect of water on lattice thermal conductivity of ringwoodite and its implications for the thermal evolution of descending slabs. Geophys. Res. Lett. 47 (13), e2020GL087607. https://doi.org/10.1029/2020GL087607.

- Mei, S., Kohlstedt, D.L., 2000. Influence of water on plastic deformation of olivine aggregates: 2. Dislocation creep regime. J. Geophys. Res. 105 (B9), 21471–21481. https://doi.org/10.1029/2000JB900180.
- Mohiuddin, A., Karato, S.I., Girard, J., 2020. Slab weakening during the olivine to ringwoodite transition in the mantle. Nat. Geosci. 13 (2), 170–174. https://doi.org/ 10.1038/s41561-019-0523-3.
- Morishima, H., Kato, T., Suto, M., Ohtani, E., Urakawa, S., Utsumi, W., Shimomura, O., Kikegawa, T., 1994. The phase boundary between α -and β -Mg₂SiO₄ determined by in situ X-ray observation. Science 265 (5176), 1202–1203. https://doi.org/10.1126/science.265.5176.1202.
- Nishi, M., Irifune, T., Gréaux, S., Tange, Y., Higo, Y., 2015. Phase transitions of serpentine in the lower mantle. Phys. Earth Planet. Inter. 245, 52–58. https://doi. org/10.1016/j.pepi.2015.05.007.
- Ohtani, E., Mizobata, H., Yurimoto, H., 2000. Stability of dense hydrous magnesium silicate phases in the systems Mg₂SiO₄-H₂O and MgSiO₃-H₂O at pressures up to 27 GPa. Phys. Chem. Miner. 27, 533–544. https://doi.org/10.1007/s002690000097.
- Ohtani, E., Toma, M., Litasov, K., Kubo, T., Suzuki, A., 2001. Stability of dense hydrous magnesium silicate phases and water storage capacity in the transition zone and lower mantle. Phys. Earth Plan. Inter. 124 (1–2), 105–117. https://doi.org/10.1016/S0031-9201(01)00192-3.
- Ohtani, E., Ishii, T., 2024. Role of water in dynamics of slabs and surrounding mantle. Prog. Earth. Planet. Sci. 11 (1), 1–20.
- Omori, S., Komabayashi, T., Maruyama, S., 2004. Dehydration and earthquakes in the subducting slab: empirical link in intermediate and deep seismic zones. Phys. Earth Planet. Inter. 146 (1–2), 297–311. https://doi.org/10.1016/j.pepi.2003.08.014.
- Pawley, A.R., McMillan, P.F., Holloway, J.R., 1993. Hydrogen in stishovite, with implications for mantle water content. Science 261 (5124), 1024–1026. https://doi. org/10.1126/science.261.5124.1024.
- Peacock, S.M., 2001. Are the lower planes of double seismic zones caused by serpentine dehydration in subducting oceanic mantle? Geology. 29 (4), 299–302. https://doi. org/10.1130/0091-7613(2001)029<0299:ATLPOD>2.0.CO;2.
- Perrillat, J.P., Chollet, M., Durand, S., van De Moortele, B., Chambat, F., Mezouar, M., Daniel, I., 2016. Kinetics of the olivine–ringwoodite transformation and seismic attenuation in the Earth's mantle transition zone. Earth Planet. Sci. Lett. 433, 360–369. https://doi.org/10.1016/j.epsl.2015.11.013.

- Purevjav, N., Fei, H., Ishii, T., Criniti, G., Lin, Y., Mao, H.K., Katsura, T., 2024.
 Temperature dependence of H₂O solubility in Al-free stishovite. Geophys. Res. Lett. 51 (3), e2023GL104029. https://doi.org/10.1029/2023GL104029.
- Rosa, A.D., Sanchez-Valle, C., Nisr, C., Evans, S.R., Debord, R., Merkel, S., 2013. Shear wave anisotropy in textured phase D and constraints on deep water recycling in subduction zones. Earth Planet. Sci. Lett. 377, 13–22. https://doi.org/10.1016/j. epsl. 2013.06.036
- Rosa, A.D., Sanchez-Valle, C., Wang, J., Saikia, A., 2015. Elasticity of superhydrous phase B, seismic anomalies in cold slabs and implications for deep water transport. Phys. Earth Planet. Inter. 243, 30–43. https://doi.org/10.1016/j.pepi.2015.03.009.
- Seaman, S.J., Williams, M.L., Jercinovic, M.J., Koteas, G.C., Brown, L.B., 2013. Water in nominally anhydrous minerals: implications for partial melting and strain localization in the lower crust. Geology. 41 (10), 1051–1054. https://doi.org/ 10.1130/G34435.1.
- Seno, T., Yamanaka, Y., 1996. Double seismic zones, compressional deep trench-outer rise events, and superplumes. Geophysic. Monograph Ser. 96, 347–355. https://doi. org/10.1029/GM096p0347.
- Shirey, S.B., Wagner, L.S., Walter, M.J., Pearson, D.G., van Keken, P.E., 2021. Slab transport of fluids to deep focus earthquake depths—Thermal modeling constraints and evidence from diamonds. AGU Adv. 2 (2), e2020AV000304. https://doi.org/ 10.1029/2021AV000434.
- Smyth, J.R., Frost, D.J., Nestola, F., Holl, C.M., Bromiley, G., 2006. Olivine hydration in the deep upper mantle: effects of temperature and silica activity. Geophys. Res. Lett. 33 (15). https://doi.org/10.1029/2006GL026194.
- Sung, C.M., Burns, R.G., 1976. Kinetics of the olivine→ spinel transition: implications to deep-focus earthquake genesis. Earth Planet. Sci. Lett. 32 (2), 165–170. https://doi.org/10.1016/0012-821X(76)90055-8.
- Tsutsumi, Y., Sakamoto, N., Hirose, K., Tagawa, S., Umemoto, K., Ohishi, Y., Yurimoto, H., 2024. Retention of water in subducted slabs under core-mantle boundary conditions. Nat. Geosci. 17, 697–704. https://doi.org/10.1038/s41561-024-01464-8.
- Zahradnik, J., Čížková, H., Bina, C.R., Sokos, E., Jánský, J., Tavera, H., Carvalho, J., 2017. A recent deep earthquake doublet in light of long-term evolution of Nazca subduction. Sci. Rep. 7 (1), 45153. https://doi.org/10.1038/srep45153.
- Zhan, Z., 2020. Mechanisms and implications of deep earthquakes. Annu. Rev. Earth Planet. Sci. 48 (1), 147–174. https://doi.org/10.1146/annurev-earth-053018-060314.